Science and Technology Indonesia
e-ISSN:2580-4391 *p*-ISSN:2580-4405
Vol. 11, No. 4, October 2026

Research Paper

Rapid and Sensitive Gold Nanoparticles Based Colorimetric Sensor for Mn(II) Ions Detection: A Potential Approach for Urinary Health Monitoring

Hanim Istatik Badi'ah[1*], Shinta Wulansari[2], Ulfatun Hasanah[3]

[1]*Department of Chemical Engineering, Faculty of Engineering, Universitas Pembangunan Nasional "Veteran", Surabaya, East Java, 60294, Indonesia*
[2]*Biotechnology Study Program, Faculty of Food Security, Universitas Negeri Surabaya, Surabaya, East Java, 60231, Indonesia*
[3]*Department of Chemistry, Faculty of Science and Technology, Universitas Annuqayah, Madura, East Java, 69463, Indonesia*
***Corresponding author**: hanim_istatik.tk@upnjatim.ac.id

Abstract
Manganese (Mn) is an essential trace element, but excessive accumulation in the human body can cause severe neurotoxic effects, making sensitive monitoring in biological fluids such as urine important for public health. This study reports a rapid colorimetric sensor based on ethylenediaminetetraacetic acid (AuNPs-EDTA) for selective Mn(II) detection. AuNPs were synthesized by chemical reduction of $HAuCl_4$ using $NaBH_4$, producing spherical nanoparticles with a surface plasmon resonance (SPR) peak at 525 nm and a size of 20-40 nm. EDTA functionalization was confirmed by an SPR red shift to 535 nm, a zeta potential change from -32.34 to -45.68 mV, FTIR spectral shifts of carboxylate and hydroxyl groups, and retention of spherical morphology with a size of 25-40 nm. Upon addition of Mn(II), the AuNPs-EDTA suspension exhibited a concentration depend on color change from wine red to blue accompanied by an LSPR shift from 535 to 670 nm. This sensor showed good linearity over 0.5 – 7.0 μg/L Mn(II) (R^2 = 0.9905), with a limit of detection (LOD) of 0.392 μg/L and a limit of quantification (LOQ) of 1.189 μg/L. High selectivity was obtained against common urinary ions and interferents, including Na^+, K^+, Ca^{2+}, Mg^{2+}, Zn^{2+}, Cu^{2+}, Pb^{2+}, Cd^{2+}, Co^{2+}, Ni^{2+}, Fe^{2+}, Cl^-, urea, uric acid, and creatinine. Recovery values of 94.46-98.01% (RSD < 2%) were achieved in spiked urine samples. These results demonstrate that AuNPs-EDTA provides a rapid, cost effective and promising platform for urinary Mn(II) monitoring.

Keywords
Gold Nanoparticles (AuNPs), EDTA, Colorimetric Sensor, Manganese Detection, Urinary Health Monitoring

Received: 15 April 2026, Accepted: 17 July 2026
https://doi.org/10.26554/sti.2026.11.4.1344-1359

1. INTRODUCTION

Manganese (Mn) is a biologically essential trace element whose excessive accumulation in human body, particularly in the central nervous system, leads to severe neurotoxicity termed manganism, manifesting as cognitive impairment, psychiatric disturbances, and Parkinsonian motor symptoms (Levy and Nassetta, 2003; Li and Yang, 2018). Despite its physiological importance in bone development, neurological function and immune regulation, Mn exhibits a narrow therapeutic window, and excessive exposure leads to severe adverse health outcomes. Chronic Mn accumulation in the central nervous system is associated with a neurodegenerative syndrome termed manganism, characterized by cognitive impairment, psychiatric disturbances, and Parkinsonian motor symptoms (Levy and Nassetta, 2003). High-risk populations include industrial workers, miners, and welders who are occupationally exposed to manganese-containing fumes and dust at concentrations that may substantially exceed regulatory thresholds. Urinary manganese in healthy, non-occupationally exposed adults is typically reported below 1.0 μg/L (geometric mean 0.7 μg/L), with population-based surveys reporting a mean of approximately 0.19 μg/L, frequently at or below the limit of detection, while occupationally exposed workers exhibit substantially elevated urinary Mn levels averaging 3.8-4.9 μg/L (Karyakina et al., 2022; Politis et al., 2021). In Indonesia, Mn contamination in groundwater has been documented at concentrations reaching up to 1.80 mg/L in East Java and between 0.991 and 2.809 mg/L in North Sumatra, far exceeding the WHO and national permissible limit of 0.1 mg/L (Putri et al., 2025; Sholehhudin et al., 2021). Biomonitoring data further underscore this concern, with blood manganese levels in welders reported to be significantly elevated compared to unexposed controls (Ramzani et al., 2022). These findings collectively highlight the urgent need for accurate, sensitive, and timely detection of Mn(II) in biological matrices, particularly urine, for both clinical and occupational health surveillance.

Conventional analytical techniques for Mn quantification in

biological fluids include atomic absorption spectroscopy (AAS), inductively coupled plasma mass spectrometry (ICP-MS), and X-ray fluorescence (XRF) (Chubarov, 2023; Kasmiati et al., 2020; Kopru and Soylak, 2024). Although these methods provide exceptional sensitivity, with ICP-MS demonstrating detection of manganese in serum down to 0.11 μg/L (Laur et al., 2020), they are inherently constrained by their reliance on expensive instrumentation, sophisticated laboratory infrastructure, time-consuming sample preparation, and the requirement for highly trained technical personnel. Such limitations render conventional methods unsuitable for resource limited settings, point-of-care (PoC) applications, or on-site occupational health screening programs. There is therefore a pressing demand for alternative detection strategies that are rapid, cost-effective, portable, and capable of delivering clinically meaningful sensitivity and selectivity at the trace concentrations characteristic of urinary manganese.

Considerable research effort has been directed toward developing alternative sensing platforms for heavy metal ion detection in biological samples. Gold nanoparticle (AuNPs)-based colorimetric sensors have attracted significant attention owing to their localized surface plasmon resonance (LSPR) properties, which produce a distance dependent color change from wine-red to blue upon nanoparticle aggregation, enabling naked eye detection without specialized instrumentation (Junaidi et al., 2024; Saha et al., 2012). AuNPs-based sensors functionalized with selective ligands and chelating agents have been successfully applied for colorimetric detection of lead, cadmium, mercury, and copper (Cai et al., 2024; Gan et al., 2020; Nadolski et al., 2023; Sengan et al., 2020), while bimetallic AuNPs platforms have further demonstrated utility in electrochemical sensing of target analytes in complex matrices such as cosmetics (Riyanto et al., 2025). Among chelating agents, ethylenediaminetetraacetic acid (EDTA) offers exceptional metal ion binding capability and has been successfully employed to functionalize AuNPs for colorimetric detection of creatinine and formalin, confirming its versatility as a surface recognition element (Saputra, 2024; Sultana et al., 2025). Paper-based microfluidic platforms (μPAD) integrating functionalized nanoparticles have further demonstrated field-deployable colorimetric detection capability for target analytes in environmental and biological matrices (Gusrizal et al., 2026). In parallel, the synthesis and characterization of metal oxide nanoparticles from coordination complex precursors has established that systematic control of synthesis parameters is critical for achieving well-defined nanomaterial properties suited to sensing applications (Raji and Bader, 2024).

A few researchers have focused on colorimetric detection of Mn(II) ions using nanoparticle-based platforms, including dopa-functionalized AuNPs Narayanan and Park (2014) reported dopa functionalized AuNPs for Mn(II) colorimetric sensing and PVP-capped silver nanoparticles (AgNPs) for Mn(II) detection in aqueous systems (Pandey et al., 2025). However, both studies primarily focused on proof-of-concept detection in simple laboratory media and never been applied to biological matrices, especially urine. Furthermore, the recognition ligands employed in previous studies were not specifically designed to exploit the strong chelation chemistry of EDTA toward Mn(II), which can provide controlled interparticle crosslinking and enhanced sensing selectivity. As far as we know, no previous study has reported an EDTA functionalized AuNPs probe for Mn(II) determination in urine with relevant of range concentration and comprehensive analytical validation, including selectivity against urinary constituents and recovery assessment in urine spiked samples. Therefore, the novelty of this research lies in: (i) the functionalization of these nanoparticles is EDTA for AuNPs-EDTA sensing probe, (ii) the development of AuNPs-EDTA colorimetric sensor specifically developed and analytically validated for Mn(II) detection in the context for potential urinary biomonitoring rather than conventional aqueous model systems, and (iii) the comprehensive validation of analytical performance for potential point of care urinary manganese monitoring application.

2. EXPERIMENTAL SECTION

2.1 Materials

All chemicals used in this study were of analytical grade and used without further purification unless otherwise stated. Chloroauric acid ($HAuCl_4$, ≥99.9%), sodium borohydride ($NaBH_4$, ≥98%), and sodium citrate tribasic dihydrate ($Na_3C_6H_5O_7{\cdot}2H_2O$, ≥99%) were obtained from Merck (Darmstadt, Germany). Ethylenediaminetetraacetic acid (EDTA, disodium salt dihydrate, ≥99%) and a certified Mn(II) standard solution (1000 mg/L in 2% HNO_3) were procured from Sigma-Aldrich (St. Louis, MO, USA). All solutions were prepared using ultrapure deionized water (resistivity ≥18.2 MΩ·cm) obtained from a Milli-Q purification system (Merck Millipore, USA). Mn(II) working standard solutions at various concentrations were freshly prepared by serial dilution of the certified stock solution prior to each experiment. All reagents were stored under appropriate conditions as specified by the respective manufacturers.

2.2 Synthesis of Gold Nanoparticles (AuNPs)

Gold nanoparticles were synthesized via a chemical reduction method based on the reduction of tetrachloroauric acid ($HAuCl_4$) using sodium borohydride ($NaBH_4$) as the primary reducing agent and sodium citrate as a stabilizing capping agent, adapted from established protocols with modifications (Frens, 1973; Turkevich et al., 1951). Briefly, 10 mL of aqueous $HAuCl_4$ solution and 10 mL of 2.0 mM sodium citrate solution was combined in a clean glass beaker under continuous magnetic stirring at room temperature. Subsequently, 10 mL of ice-cold 1.0 mM $NaBH_4$ solution was added dropwise to the mixture while stirring was maintained. The immediate reduction of Au(III) to Au(0) was evidenced by a color transition of the solution from pale yellow to deep wine-red, indicative of the formation of colloidal AuNPs and the characteristic excitation of the surface plasmon resonance (SPR) band. Stirring was continued for an additional 10 minutes to ensure complete reaction. The resulting AuNPs colloids were subsequently cen-

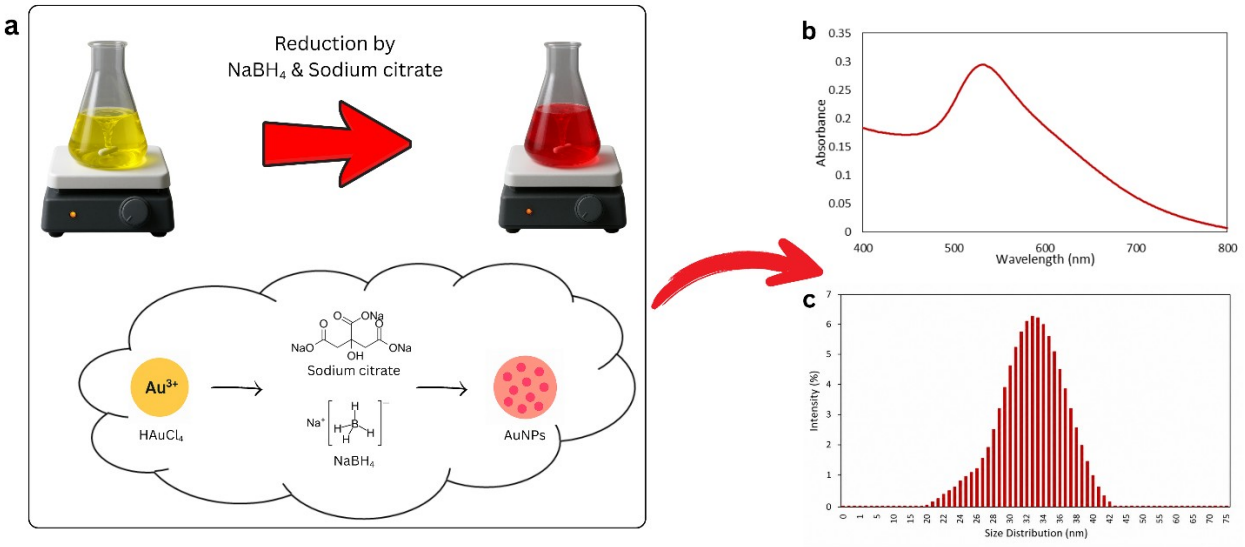

Figure 1. Schematic Representation of AuNPs (a) Synthesis Mechanism, (b) UV-Visible Absorption Spectra, (c) Size Distribution

trifuged at 10,000 rpm for 15 minutes and filtered through a 0.45 μm membrane filter to remove unreacted reagents and aggregates. The purified AuNPs suspensions were stored in amber glass vials at 4 °C until further use.

To systematically investigate the effect of precursor concentration on nanoparticle properties, $HAuCl_4$ concentrations of 0.50; 0.75; 1.00; 1.50; and 2;00 mM were evaluated while all other synthesis parameters were held constant. The $HAuCl_4$ concentration is a critical determinant of AuNPs nucleation kinetics and growth dynamics, which directly influence particle size, monodispersity, and optical properties including the position and intensity of the SPR absorption band (Taha and Shamsuddin, 2014).

2.3 Surface Modification of AuNPs with EDTA (AuNPs-EDTA)

Surface functionalization of AuNPs with EDTA was performed to introduce chelating moieties capable of selectively binding Mn(II) ions. A solution of 0.5% (w/v) EDTA was prepared in deionized water and its pH was adjusted to 7.0 using 0.1 M NaOH to ensure optimal chelation conditions. A total of 10.0 mL of the prepared EDTA solution was added dropwise to 30.0 mL of purified AuNP suspension under continuous stirring at room temperature, yielding a 3:1 (v/v) AuNPs:EDTA volume ratio. The mixture was subsequently subjected to probe ultrasonication at a frequency of 20 kHz for 10 minutes to promote uniform adsorption of EDTA molecules onto the AuNP surface and to disrupt any nascent aggregates. Following sonication, the EDTA-functionalized AuNPs (EDTA-AuNPs) were centrifuged at 12.000 rpm for 15 minutes to pellet the functionalized nanoparticles. The supernatant was carefully decanted, and the pellet was resuspended in an equal volume of deionized water. This washing step was repeated twice to remove unbound EDTA. The resulting EDTA-AuNPs were characterized by UV-Vis spectroscopy, particle size analysis (PSA), and transmission electron microscopy (TEM).

2.4 Physicochemical Characterization of AuNPs-EDTA

The optical properties of both AuNPs unmodified and AuNPs-EDTA were characterized using a UV-Vis spectrophotometer (Thermo Scientific Genesys 10S, USA) over a wavelength range of 400–800 nm, with deionized water as the reference blank. The position and full-width at half-maximum (FWHM) of the SPR absorption band were recorded to assess nanoparticle formation, surface modification, and colloidal stability. Hydrodynamic diameter, polydispersity index (PDI), and zeta potential were measured using dynamic light scattering (DLS) with a Zetasizer Nano ZS instrument (Malvern Instruments, ver. 7.01, Germany). Measurements were performed in triplicate at 25°C. The morphology and core size distribution of the synthesized nanoparticles were examined by transmission electron microscopy (TEM) using a JEOL JEM-2100Plus microscope operating at an accelerating voltage of 200 kV. TEM samples were prepared by depositing 5 μL of the nanoparticle suspension onto a 300-mesh carbon-coated copper grid and allowing it to air-dry at room temperature prior to imaging. Representative TEM micrographs were analyzed using ImageJ software (National Institutes of Health, USA) to estimate mean particle diameter and evaluate size distribution histograms from a minimum of 100 individual nanoparticles of sample. The functional group of AuNPs, EDTA, and AuNPs-EDTA were identifying with FTIR spectrophotometer (400-4000 cm^{-1}) to confirm EDTA immobilization on the AuNPs surface. In this research, an analysis of zeta potential was also carried out

Table 1. Summary of Analytical Performance Parameters of AuNPs-EDTA Colorimetric Sensor for Mn(II) Detection

Parameter	Value/Range	Method/Standard
Linear range	0.5 – 7.0 μg/L	Calibration curve
Correlation coefficient (R^2)	0.9905	Linear regression
LOD	0.392 μg/L	IUPAC guidelines
LOQ	1.189 μg/L	IUPAC guidelines
Precision	<5%	Triplicate measurement
Selectivity	Na^+, K^+, Ca^{2+}, Mg^{2+}, Zn^{2+}, Cu^{2+}, Pb^{2+}, Cd^{2+}, Co^{2+}, Ni^{2+}, Fe^{3+}, urea, uric acid, and creatinin	Signal deviation ±5%
Incubation time	5 minutes	Room temperature (25°C)
Detection method	UV-Vis (400–800 nm)	Absorbance ratio A_{670}/A_{535}

to determine the colloidal stability.

2.5 Colorimetric Detection of Mn(II) Ions Using AuNPs-EDTA

The colorimetric sensing performance of the AuNPs-EDTA probe toward Mn(II) ions was evaluated through a systematic mixing protocol. Mn(II) working solutions at specified concentrations were freshly prepared by serial dilution of the certified 1000 mg/L stock standard. The pH of this detection was maintained at pH 7.0 using phosphate buffer, that EDTA will be chelating capacity at pH 7.0 (Al Sheidi et al., 2024), and pH optimization study is planned as future work. For each measurement, 1.0 mL of AuNPs-EDTA suspension was pipetted into a clean microcentrifuge tube and mixed with 1.0 mL of Mn(II) solution at the target concentration. The mixture was vortexed for 10 seconds to ensure homogeneous mixing and allowed to incubate at room temperature (25 ± 1 °C) for 5 minutes to permit Mn(II)-AuNPs-EDTA interaction and nanoparticle aggregation to proceed to equilibrium. Colorimetric responses were first assessed by naked-eye visual observation under ambient lighting conditions. The UV-Vis absorption spectra of the resulting mixtures were then recorded over the wavelength range of 400–800 nm. The ratio of absorbance at the aggregation peak (650–700 nm) to the original SPR peak was used as the primary analytical signal as A_{670}/A_{535}, to construct calibration relationships, minimizing variability attributable to instrument drift or concentration fluctuations.

2.6 Analytical Performance and Method Validation

The analytical performance of the AuNPs-EDTA colorimetric sensor was evaluated according to ICH Q2(R1) and IUPAC guidelines for method validation, encompassing linearity, sensitivity, limit of detection (LOD), limit of quantification (LOQ), precision, and selectivity.

Linearity was established by constructing calibration curves over a range of Mn(II) standard concentrations from 0.5 to 7.0 µg/L (urinary manganese in healthy, non-occupationally exposed adults is typically reported below 1.0 μg/L) (Politis et al., 2021), with the absorbance ratio (A_{670}/A_{535}) plotted as a function of Mn(II) concentration. The Pearson correlation coefficient (R^2) was calculated to assess the quality of the linear fit. Sensitivity was derived from the slope of the linear regression equation, reflecting the change in analytical signal per unit change in analyte concentration. The LOD and LOQ were calculated according to the following Equations (1) and (2).

$$LOD = 3.3 \times (SD/S) \quad (1)$$

$$LOQ = 10 \times (SD/S) \quad (2)$$

where SD is the standard deviation of the response of the blank or lowest detectable standard concentration, and S is the slope of the calibration curve. Precision was assessed by performing all measurements in triplicate (n = 3) and reporting intra-assay relative standard deviation (RSD%).

Selectivity of the AuNPs-EDTA sensor toward Mn(II) was evaluated by examining the colorimetric response in the presence of common co-existing cations likely to be encountered in biological matrices, particularly urine. The following potential interferents were individually tested at physiologically and analytically relevant concentrations: sodium (Na+), potassium (K^+), calcium (Ca^{2+}), magnesium (Mg^{2+}), zinc (Zn^{2+}), copper (Cu^{2+}), lead (Pb^{2+}), cadmium (Cd^{2+}), cobalt (Co^{2+}), nickel (Ni^{2+}), iron (Fe^{3+}), urea, uric acid, and creatinin. The selectivity was assessed by comparing the absorbance ratio obtained in the presence of each interfering ion against that obtained with Mn(II) alone, and calculating the percentage signal deviation. An interfering ion was considered non-significant if the signal deviation was within ±5% relative to the Mn(II) response. The summary of analytical performance parameters shown at Table 1, like a linear range, correlation coefficient (R^2), LOD, LOQ, precision, selectivity, and incubation time.

3. RESULTS AND DISCUSSIONS

3.1 Synthesis and Optical Characterization of AuNPs

Gold nanoparticles (AuNPs) were successfully synthesized via a chemical reduction approach using $NaBH_4$ as a strong reducing

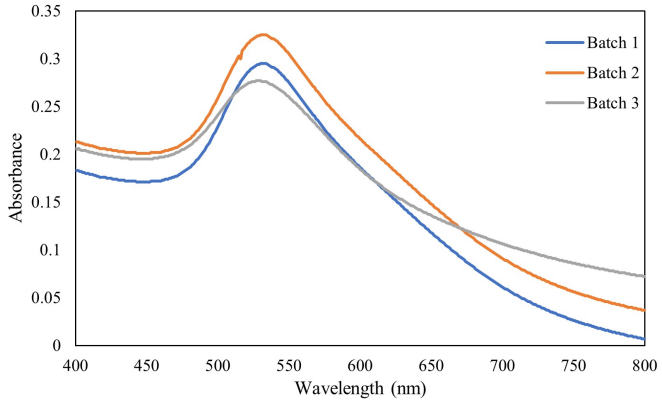

Figure 2. UV-Visible Spectra of Batch to Batch AuNPs Synthesis

Table 2. Batch to Batch Reproducibility of AuNPs Synthesis Process

Parameter	λ max	Absorbance
Batch 1	530	0.295
Batch 2	535	0.325
Batch 3	528	0.277

agent for the conversion of Au(III) precursor ($HAuCl_4$) to zerovalent metallic gold (Au0), with sodium citrate serving as an electrostatic stabilizer. The formation of AuNPs was immediately confirmed by a sharp, visually perceptible color transition of the reaction solution from pale yellow that characteristic of the [$AuCl_4$] complex to a deep wine-red coloration, a hallmark of colloidal gold indicative of the excitation of the localized surface plasmon resonance (LSPR) effect. This phenomenon arises from the coherent collective oscillation of conduction band electrons at the nanoparticle surface in resonance with the incident electromagnetic radiation, producing a strong absorption band in the visible region (Turkevich et al., 1951). The reduction of Au^{3+} to Au0 by $NaBH_4$ proceeds via a rapid electron-transfer mechanism, with sodium citrate subsequently adsorbing onto the nascent nanoparticle surface through electrostatic interaction, imparting a negative surface charge that prevents particle coalescence through interparticle electrostatic repulsion (Frens, 1973).

UV-Vis spectrophotometric analysis confirmed the formation of AuNPs by revealing a pronounced absorption maximum centered at 530 nm, as shown in Figure 1, corresponding to the characteristic SPR band of spherical gold nanoparticles. This absorption range is in excellent agreement with the theoretically predicted and experimentally reported SPR peak position for citrate-capped spherical AuNPs in the size range of 10–50 nm (Shamsuddin et al., 2020; Taha and Shamsuddin, 2014). The sharpness and symmetry of the SPR peak indicate a relatively narrow size distribution and high colloidal stability of the synthesized nanoparticles, consistent with previous reports on $NaBH_4$-reduced AuNPs stabilized by citrate (Butt et al., 2025). A sharp, well-defined SPR absorption peak at approximately 520–540 nm is widely regarded as diagnostic evidence for the successful formation of monodisperse, stable colloidal AuNPs (Saffee et al., 2019). Importantly, the absence of secondary absorption bands at longer wavelengths (>600 nm) in the optimized preparation confirms that inter-particle aggregation was minimal and that the synthesized colloids were in a well-dispersed state. To evaluate the reproducibility of the synthesis procedure, AuNPs were independently prepared in three separate batches under identical experimental conditions. The UV-Vis spectra of all batches (Table 2 and Figure 2) exhibited highly similar surface plasmon resonance (SPR) peaks, with λ max values of 530, 535, and 528 nm, respectively. The mean SPR wavelength was 531 nm with a standard deviation (SD) of 5.09 nm and a relative standard deviation (RSD) of 0.57%. The low RSD value indicates a good batch to batch reproducibility and demonstrated that the synthesis protocol consistently produces AuNPs with comparable optical properties.

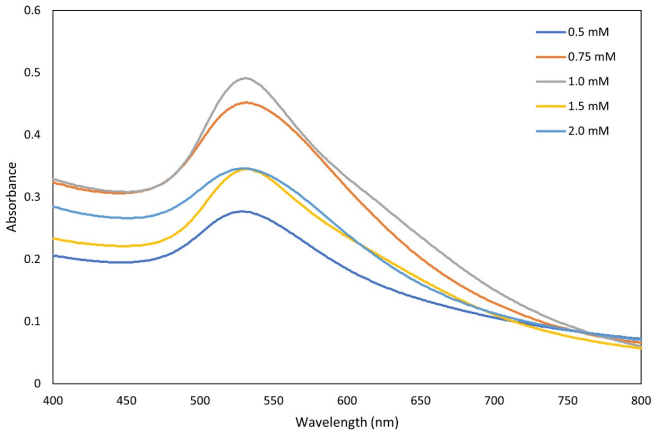

Figure 3. UV-Visible Absorption Spectra of AuNPs Upon the Addition of Different HAuCl4 Concentration

Particle size analysis (PSA) revealed that the hydrodynamic diameter of the synthesized AuNPs ranged from 20 to 40 nm, with a polydispersity index (PDI) of less than 0.5, confirming a narrow and homogeneous size distribution consistent with a monodisperse colloidal system. The PDI value below 0.5 is an accepted criterion for classifying nanoparticle suspensions as sufficiently monodisperse for sensing applications, as size uniformity is a critical determinant of the reproducibility and magnitude of the colorimetric response (Osibe and Aoyagi, 2019). The size dependent optical properties of AuNPs are well established, smaller and more uniform particles produce sharper, more intense SPR peaks, which directly translates to higher sensitivity and a more pronounced colorimetric signal upon analyte-induced aggregation (Shamsuddin et al., 2020). The obtained particle size range of 20-40 nm is therefore

Table 3. Zeta Potential and PDI Results of AuNPs Unmodified and AuNPs-EDTA

Sample	Z-Average (nm)	PDI	Zeta Potential (%)
AuNPs unmodified	50	0.49	-32.23
AuNPs-EDTA	54	0.36	-45.68

consistent with effective colorimetric probe design for metal ion detection.

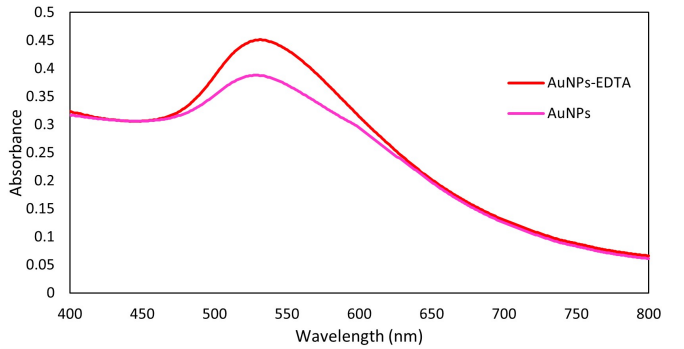

Figure 4. UV-Visible Absorption Spectra of AuNPs Colloidal and AuNPs-EDTA

3.2 Effect of $HAuCl_4$ Precursor Concentration of AuNPs Synthesis

The influence of $HAuCl_4$ precursor concentration on the optical and physicochemical properties of the synthesized AuNPs was systematically investigated over the range of 0.50, 0.75, 1.00, 1.50, and 2.00 mM, with all other synthesis parameters held constant. The $HAuCl_4$ concentration plays a pivotal role in governing both the nucleation kinetics and the subsequent growth dynamics of AuNPs, thereby exerting a direct influence on particle size, morphology, colloidal stability, and the position and intensity of the SPR absorption band (Vigneshvar et al., 2016). Understanding this concentration-dependent behavior is essential for rationally optimizing AuNPs properties toward specific sensing applications.

At the lowest precursor concentration of 0.50 mM, UV-Vis spectrophotometric analysis revealed a relatively low absorbance intensity at the SPR peak (520 nm), indicative of a limited nucleation yield and the formation of smaller-sized nanoparticles with a lower total gold content per unit volume. This observation is consistent with the expectation that, at low $HAuCl_4$ concentrations, the available gold ions are insufficient to sustain extensive particle growth beyond the initial nucleation stage, yielding a relatively dilute colloidal suspension of small nanoparticles (Saha et al., 2012). Upon increasing the HAuCl4 concentration to 0.75 mM, a marked enhancement in SPR absorbance intensity was observed, accompanied by a slight red-shift of the absorption maximum to approximately 526 nm. This bathochromic shift reflects an increase in mean particle diameter, as larger AuNPs possess a higher polarizability and exhibit an SPR maximum at longer wavelengths in accordance with Mie scattering theory (Turkevich et al., 1951).

The $HAuCl_4$ concentration of 1.00 mM yielded the most favorable synthesis outcome, producing an SPR band centered at approximately 530 nm with the highest absorbance intensity and the sharpest peak profile among all concentrations tested, as shown in Figure 3. These spectral characteristics was high peak intensity, narrow bandwidth, and a well-defined absorption maximum in the 520–535 nm range, are collectively indicative of optimal nanoparticle formation: high yield, uniform particle size, and excellent colloidal mono dispersity (Taha and Shamsuddin, 2014). The colloidal suspension produced at 1.00 mM $HAuCl_4$ exhibited minimal visible aggregation and maintained its characteristic wine-red color over an extended period, confirming its superior colloidal stability. This concentration was therefore selected as the optimal $HAuCl_4$ concentration for subsequent AuNPs synthesis in all further experiments. The selection of 1.00 mM $HAuCl_4$ as the optimal precursor concentration is corroborated by previous literature reports Turkevich et al. (1951) and Frens (1973) established the foundational relationship between gold precursor concentration and particle size in citrate reduction systems (Frens, 1973; Turkevich et al., 1951), while more recent studies have consistently demonstrated that intermediate $HAuCl_4$ concentrations in the range of 0.5 - 1.0 mM yield the most monodisperse and colloidally stable AuNPs (Saha et al., 2012).

At elevated precursor concentrations of 1.50 and 2.00 mM, a pronounced broadening of the SPR absorption band and a concomitant decrease in peak absorbance intensity were observed. These spectral features are characteristic of nanoparticle aggregation and polydispersity, arising from the destabilization of the colloidal suspension when the gold ion concentration exceeds the stabilizing capacity of the citrate capping layer (Vigneshvar et al., 2016). At high $HAuCl_4$ concentrations, the excess gold ions compete with the stabilizing citrate anions for surface binding sites, reducing the effective electrostatic repulsion between particles and promoting interparticle coalescence. The resulting aggregated AuNPs exhibit a red-shifted and broadened SPR band that consistent with the well-documented aggregation-induced plasmon coupling phenomenon and a visually perceptible color shift from wine-red toward blue-grey. These findings collectively establish 1.00 mM as the optimal HAuCl4 concentration, representing the critical balance between sufficient gold ion supply for high-yield nanoparticle formation and adequate citrate-mediated colloidal stabilization.

Table 4. Comparison of the Analytical Performance of AuNPs-EDTA with Recently Reported Mn(II) Detection Methods

Method	Material	Sample Matrix	LOD (μg/L)	Reference
AAS	AAS method	Waste Water Treatment (IPAL)	0.4287 g/ml or 428700000 μg/L	(Kasmiati et al., 2020)
Fluorescence	His-CQDs	Whole blood	1.85 μg/L	(Mohagheghpour et al., 2022)
μ-PAD	Microfluidic paper	Natural water	26 μg/L	(Nitti et al., 2023)
Electrochemical	Gold electrode	Drinking water	4.64 μM	(Lamothe et al., 2024)
Colorimetric	TRPIDA V-AuNPs	Environmental water	6.9 μg/L	(Shange et al., 2025)
Colorimetric	Solid-phase extraction	Water	50 μg/L	(Kohama et al., 2025)
Colorimetric	PVP-AgNPs	Water	0.09 μg/L	(Pandey et al., 2025)
Colorimetric	AuNPs-EDTA	Spiked urine	0.392 μg/L	This work

Table 5. Recovery of Mn(II) in Spiked Urine Sample Using AuNPs-EDTA Colorimetric Sensor (n=3)

Added Concentration of Mn(II) (μg/L)	Found Concentration of Mn(II) (μg/L)	Recovery (%)	RSD (%)
1.0	0.94	94.46	0.93
3.0	2.97	98.01	1.70
5.0	4.96	97.81	1.58

3.3 AuNPs Surface Modification with EDTA (AuNPs-EDTA)

Unmodified gold nanoparticles (AuNPs) stabilized solely by citrate capping agents are inherently susceptible to aggregation in the presence of elevated ionic strength, competing cations, or biomolecular matrices, owing to the relatively weak electrostatic repulsion conferred by adsorbed citrate anions (Turkevich et al., 1951). To overcome these limitations and introduce selective metal ion recognition capability, surface modification of the synthesized AuNPs with EDTA was carried out. EDTA is a hexadentate chelating agent containing two tertiary amine nitrogen atoms (-N) and four carboxylate oxygen atoms ($-COO^-$) that serve as electron pair donors in coordinative bonding. The gold nanoparticle surface provides electron accepting sites through its d-band electrons, enabling EDTA adsorption through Au−N and Au−O coordinative interactions supplemented by electrostatic attraction between the negatively charged carboxylate groups and the partially positive gold surface at the point attachment (Amina and Guo, 2020; Pedroso-Santana and Fleitas-Salazar, 2023). After binding to the AuNPs surface, EDTA forms a protective layer that enhances the colloidal stability of the nanoparticles. This layer provides both steric and electrostatic repulsion, which helps prevent unwanted nanoparticle aggregation and maintains a stable dispersion more effectively that citrate alone (Pedroso-Santana and Fleitas-Salazar, 2023). Importantly, the EDTA molecules attached to the nanoparticle surface retain their metal chelating ability through the remaining free carboxylate and amine groups. As a result, these functional groups can interact with Mn(II) ions, enabling the AuNP-EDTA system to generate a selective colorimetric response toward Mn(II) (Ali and Azzam, 2023; Saputra, 2024).

The successful functionalization of AuNPs with EDTA was confirmed by UV-Vis spectrophotometric analysis, as shown in Figure 4. This figure shown the following EDTA functionalization, the SPR peak of AuNPs shifted from approximately 525 nm to 535 nm, corresponding to a bathochromic (red) shift of about 10 nm. This spectral change indicates a modification of the local dielectric environment surrounding the nanoparticles. According to Mie theory, the LSPR wavelength is sensitive to changes in the refractive index near the nanoparticle surface. When citrate molecules are replaced by larger EDTA molecules, the effective refractive index around the AuNPs increases, resulting in red shift of the SPR peak (Koushki, 2021). The observed shift is concistent with previous studies reporting SPR red shifts after surface functionalization of AuNPs with organic ligands. Similar wavelength shifts have been reported following antibody conjugation and EDTA modification of AuNPs, confirming that changes in the surface chemistry can significantly influence the plasmonic properties of gold nanoparticles (Potts et al., 2023; Saputra, 2024). In addition to the SPR shift, the AuNPs-EDTA spectrum exhibited a narrower absorption band compared with AuNPs unmodified. This narrowing suggests a more uniform surface environment, which is consistent with successful and relatively homogeneous EDTA coverage on the nanoparticle surface. Furthermore, no secondary absorption band was observed above 600 nm, indicating that EDTA functionalization did not induce unwanted nanoparticle aggregation. The absence of aggregation is important because it provides a stable baseline state for subsequent Mn(II) sensing experiments.

FTIR spectroscopy was employed to verify the successfully of immobilization of EDTA on the AuNPs surface by comparing the spectra of free EDTA and AuNPs-EDTA (Figure 5). In the spectrum of free EDTA, a broad absorption band at 3522.02 cm^{-1} was assigned to the overlapping O−H and N−H stretching vibrations, while a weaker band at 2998.06 cm^{-1} cor-

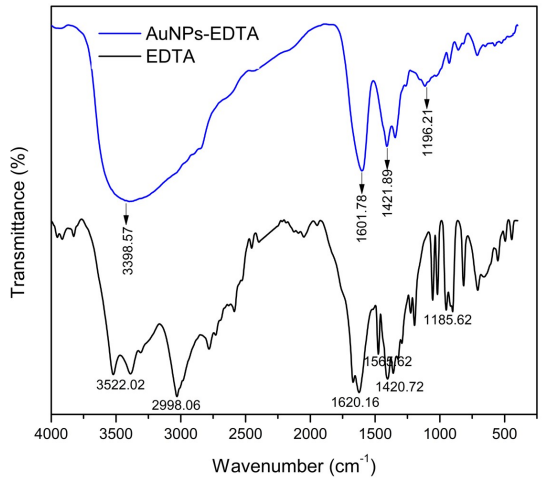

Figure 5. FTIR Spectra of AuNPs, AuNPs-EDTA, and EDTA

responded to the aliphatic C−H stretching vibration of the ethylenediamine backbone. After functionalization, these two absorption bands were no longer clearly distinguishable and appeared as a single board band extending from approximately 2800-3600 cm^{-1}. This band coalescence is most plausibly attributed to an overall broadening and merging of the O−H, N−H, and C−H stretching envelope upon surface immobilization. Such broadening is consistent with the inherently overlapping spectral ranges of these vibrational modes (C−H stretching of aliphatic groups typically occurs at 2800-3600 cm^{-1}, directly adjacent to and overlapping with O−H or N−H stretching in the 3200-3600 cm^{-1} region), and may be further amplified by an expanded hydrogen bonding network at the nanoparticle interface, involving interactions between surface bound EDTA, residual hydration water, and EDTA molecules within the surface layer.

The most significant evidence for successful EDTA functionalization is observed in the carboxylate stretching region. The asymmetric stretching vibration of the carboxylate group (ν_asym) shifted from 1620.16 cm^{-1} to 1601.78 cm^{-1} after functionalization, whereas the symmetric stretching vibration (ν_sym) remained nearly unchanged, shifting only slightly from 1420.72 cm^{-1} to 1421.89 cm^{-1}. Consequently, the separation between the asymmetric and symmetric stretching band ($\Delta\nu$ = ν_asym - ν_sym) decreased from 199.4 cm^{-1} for free EDTA to 179.9 cm^{-1} after adsorption onto the AuNPs surface. According to the Deacon-Philips criterion, change in $\Delta\nu$ are widely used to evaluate variations in the coordination environment of carboxylate groups following their interaction with metal surface (Nakamoto, 2008). The observed decrease in $\Delta\nu$ suggests that the electronic environment of the carboxylate groups was altered after EDTA immobilization, indicating that these functional groups participated in the interaction with the AuNPs surface. Although FTIR alone cannot determine the exact binding configuration of EDTA, the observed spectral changes provide strong evidence that surface adsorption occurred successfully. Reduction in carboxylate stretching frequencies reflecting changes in the chemical environment of surface bound carboxylate groups following functionalization (Sutton et al., 2015). Another notable spectral change is the disappearance of the distinct N−H bending vibration observed at 1565.62 cm^{-1} in the spectrum of free EDTA. Rather than indicating the loss of amine functional groups, this observation is more likely associated with changes in the vibrational environment of EDTA following its adsorption onto the AuNPs surface. The N−H bending region partially overlaps with the stronger carboxylate absorption bands, making the weaker N−H vibration difficult to distinguish after functionalization. In addition, adsorption onto the nanoparticle surface can modify the hydrogen bonding environment and the electron distribution around the amine groups, leading to reduced intensity or band broadening of the N−H vibration. Importantly, the slight shift of the C−N stretching vibration from 1185.62 cm^{-1} to 1196.21 cm^{-1} indicates that the ethylenediamine backbone of EDTA remained intact after functionalization. The retention of the EDTA backbone is important because it suggests that the ligand maintained its metal chelating functionality, which is essential for the subsequent interaction with Mn(II) during the colorimetric sensing process. Therefore, the disappearance of the N−H bending band not interpreted as degradation of the EDTA molecule but rather as a consequence of spectral overlap and changes in the local chemical environment.

The successful functionalization of AuNPs with EDTA also was confirmed by zeta potential measurements, as shown in Table 3. The zeta potential of AuNPs unmodified was -32.23 mV and it became more negative after EDTA functionalization, that -45.68 mV. This increase in negative charge indicates that EDTA has been successfully adsorbed onto the AuNPs surface. The corboxylate groups ($-COO^-$) from EDTA contribute additional negative charges, which strengthen electrostatic repulsion between particles and improve colloidal stability (Pedroso-Santana and Fleitas-Salazar, 2023; Sultana et al., 2025). The magnitude of the zeta potential is also an important indicator of colloidal stability. Nanoparticle dispersions with zeta potential values greater than ±30 mV was generally considered electrostatically stable because the repulsive force between particles was sufficient to overcome attractive Van der Waals interactions. Therefore, the more negative zeta potential observed after EDTA modification suggests that the AuNPs-EDTA suspension processes improved resistance to undesired aggregation compared with AuNPs unmodified. Furthermore, the PDI decrease from -0.49 to – 0.36 after modification with EDTA, indicating a narrower particle size distribution and improved dispersion homogeneity. This result suggests that the EDTA layer not only modifies the nanoparticle surface chemistry but also contributes to maintaining a more uniform colloidal system. The combined zeta potential and PDI results are consistent with the UV-Vis analysis, collectively confirming the successfully of AuNPs modified with EDTA.

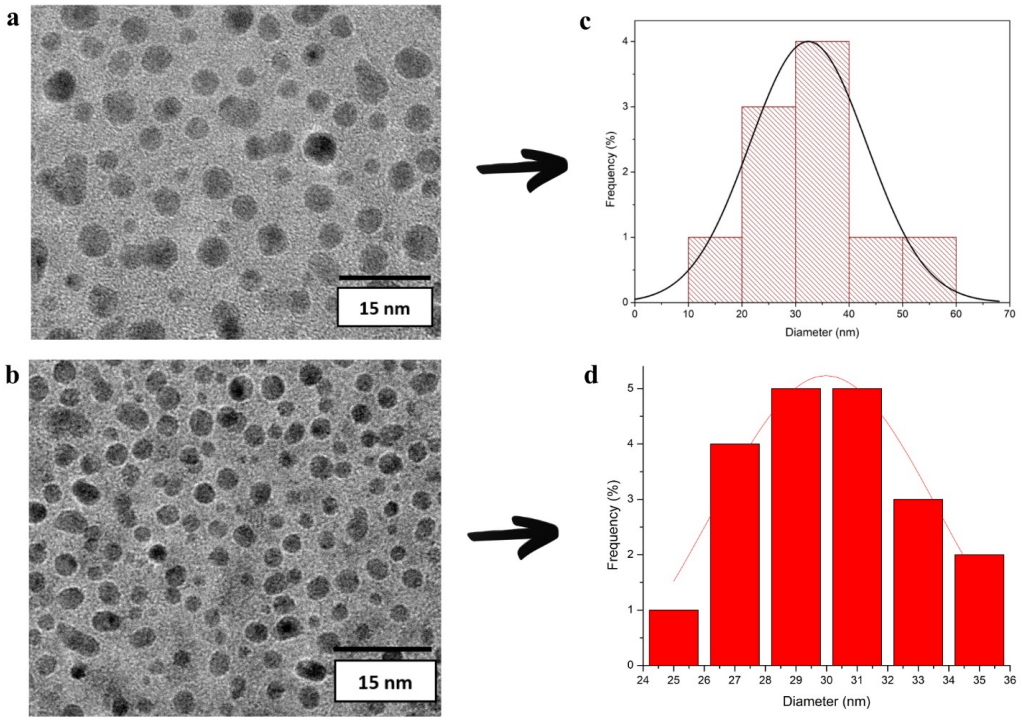

Figure 6. TEM Image of (a) AuNPs, (b) AuNPs-EDTA, Particle Size Distribution of (c) AuNPs, (d) AuNPs-EDTA

Transmission electron microscopy (TEM) was used to evaluate the morphology and size of AuNPs unmodified and AuNPs functionalized EDTA. As shown in Figure 6a, the AuNPs unmodified exhibited predominantly spherical particles with a relatively narrow size distribution and minimal particle aggregation, indicating the successfully of nanoparticle synthesis. TEM imaging (Figure 6b) demonstrated that the AuNPs-EDTA retained their well-dispersed, spherical morphology without any observable particle fusion, reshaping, or significant aggregation. This preservation of morphological integrity indicates that the EDTA modification process was sufficiently mild to avoid disrupting nanoparticle structure, and that the EDTA ligand shell effectively stabilized the nanoparticle surface against interparticle coalescence (Kusuma et al., 2023). The absence of aggregation in AuNPs-EDTA is a critical prerequisite for their function as colorimetric sensing probes: an aggregation-free baseline state ensures that any colorimetric response observed upon analyte addition is unambiguously attributable to Mn(II)-induced interparticle cross-linking rather than background aggregation (Sengan et al., 2020). The spherical morphology of AuNPs-EDTA is particularly advantageous for sensing applications, as it maximizes the available surface area per unit mass for analyte binding, thereby enhancing detection sensitivity (Kusuma et al., 2023).

Quantitative size analysis of AuNPs-EDTA was performed using ImageJ software on calibrated TEM micrographs, with a minimum of 100 individual particles measured per sample to ensure statistical significance. The resulting size distribution histogram of AuNPs unmodified (Figure 6c), the most particles were distributed within the range of approximately 20-40 nm with the highest frequency observed around 30-35 nm. Such a narrow and uniformly distribution is consistent with the nucleation growth mechanism, where rapid nucleation followed by controlled particle growth produces relatively monodisperse nanoparticle. And the histogram of AuNPs-EDTA (Figure 6d) revealed an average AuNPs-EDTA diameter in the range of 25–40 nm, with a Gaussian-shaped distribution (R^2 = 0.9280) indicating satisfactory size uniformity and a well-controlled synthesis process. This size range is consistent with PSA/DLS measurements, confirming the good agreement between hydrodynamic diameter and core diameter for spherical nanoparticles of this size class. The slightly broader size distribution observed in AuNPs-EDTA compared to AuNPs unmodified is attributable to the hydrodynamic contribution of the surface-adsorbed EDTA layer and is not indicative of particle growth or aggregation (Potts et al., 2023). The particle size range of 25-40 nm is well-suited for colorimetric sensing applications: nanoparticles in this range produce sufficiently strong LSPR absorption at 520-535 nm while remaining colloidally stable, and their aggregation upon metal ion binding generates a pronounced red-shift readily detectable by UV-Vis spectrophotometry or naked-eye observation (Potts et al., 2023).

Collectively, the UV-Vis spectrophotometric, zeta potential data, FTIR, and TEM characterization confirm that EDTA was successfully and uniformly adsorbed onto the AuNPs surface without compromising nanoparticle integrity or colloidal

stability. The surface-bound EDTA serves a dual functional role in the present sensing platform: (i) as a stabilizing capping agent that prevents non-specific aggregation through steric and electrostatic repulsion, and (ii) as a metal ion recognition element that facilitates selective complexation of Mn(II) through its carboxylate and amine coordination sites, triggering controlled interparticle aggregation and a measurable colorimetric response (Saputra, 2024). This dual functionality of EDTA-simultaneously stabilizing the probe and enabling selective analyte recognition distinguishes AuNPs-EDTA from simple citrate-stabilized probes and underpins the superior selectivity of the colorimetric sensor developed in this study. The AuNPs-EDTA were therefore confirmed as suitable, well-characterized sensing probes for the subsequent colorimetric detection of Mn(II) ions.

3.4 Colorimetric Detection of Mn(II) Ions using AuNPs-EDTA

The colorimetric detection of Mn(II) ions using AuNPs-EDTA is based on a chelation-induced interparticle crosslinking aggregation mechanism, which directly modifies the LSPR characteristics of the gold nanoparticles and produces a distinct, concentration-dependent color change observable to the naked eye. Under baseline conditions, AuNPs-EDTA are stably dispersed in aqueous solution due to the electrostatic repulsion conferred by the negatively charged carboxylate (COO^-) and amine ($-NH_2$) functional groups of the surface-bound EDTA ligands, maintaining the characteristic wine-red coloration of a well-dispersed AuNPs colloid with SPR absorption at 535 nm (Ali and Azzam, 2023). This electrostatic stabilization can be understood within the framework of the Derjaguin Landau Verwey Overbeek (DLVO) theory, in which colloidal stability is governed by the balance between attractive van der Waals forces and repulsive electrostatic double-layer interactions: so long as the surface charge density remains sufficiently high, repulsive forces dominate and aggregation is prevented (Sadiq et al., 2024).

Upon introduction of Mn(II) ions into the AuNPs-EDTA suspension, rapid chelation occurs between the Mn(II) ions and the EDTA ligands anchored on the nanoparticle surface. EDTA is a hexadentate chelating agent with an exceptionally high stability constant (log K = 13.79 for Mn-EDTA complexes), enabling it to form thermodynamically stable, octahedral coordination complexes with Mn(II) through its two nitrogen and four carboxylate oxygen donor atoms (Alpaslan et al., 2020). Critically, because each Mn(II) ion is capable of simultaneously coordinating with EDTA ligands immobilized on two or more adjacent nanoparticles, it functions as an interparticle crosslinking bridge that progressively reduces the average interparticle distance across the colloidal ensemble (Narayanan and Park, 2014; Wei et al., 2024). This crosslinking-mediated bridging mechanism is distinct from simple non-crosslinking aggregation: rather than a global destabilization of the colloidal surface charge, the EDTA–Mn(II)–EDTA bridge formation results in a controlled, stoichiometry-dependent aggregation whose extent scales with Mn(II) concentration (Sadiq et al., 2024). As the interparticle distance falls below a critical threshold, strong electromagnetic coupling between the surface plasmon fields of neighboring nanoparticles occurs a phenomenon termed interparticle plasmon coupling, which collectively shifts the LSPR absorption to longer wavelengths (Kusuma et al., 2023). However, the objective of this study was to evaluate the feasibility of EDTA as both a capping agent for AuNPs stabilization and a recognition ligand for Mn(II) detection. Based on the observed aggregation behavior and UV-Vis spectra change, an EDTA-Mn(II)-EDTA interparticle bridging pathway is proposed as a plausible explanation for the sensing response. Although, direct experimental evidence confirming the exact coordination structure was not obtained in the present study and therefore the proposed mechanism should be regarded as a working hypothesis.

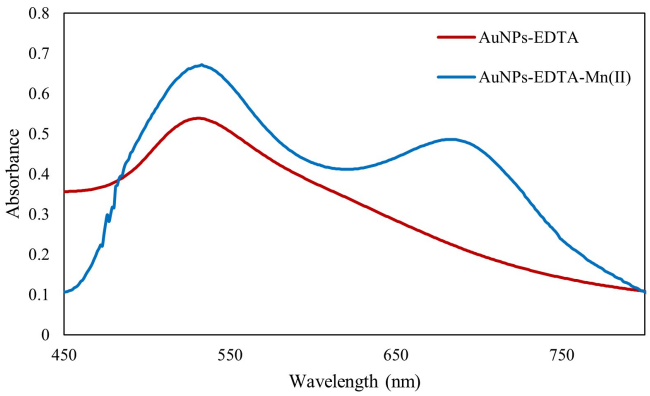

Figure 7. UV-Vis Absorption Spectra of AuNPs-EDTA, and AuNPs-EDTA in Presence of Mn(II)

The Mn(II)-induced aggregation of AuNPs-EDTA was clearly manifested in the UV-Vis absorption spectra, as shown in Figure 7. In the absence of Mn(II), the AuNPs-EDTA exhibited a sharp and symmetric SPR absorption peak at approximately 535 nm with high absorbance intensity, consistent with a well-dispersed, stable colloidal state (Taha and Shamsuddin, 2014). Upon addition of Mn(II) ions, a progressive and concentration-dependent red-shift of the SPR absorption band from 535 nm to 670 nm was observed, accompanied by a concomitant decrease in the absorbance intensity at 535 nm and the emergence and growth of a new, broad absorption band at approximately 670 nm. This spectral evolution is characteristic of plasmonic coupling between aggregated AuNPs as interparticle distances decrease due to Mn(II)-mediated crosslinking, the collective oscillation of conduction electrons across the coupled nanoparticle clusters resonates at a substantially lower frequency than that of isolated particles, yielding the observed bathochromic shift (Takayanagi et al., 2022). The magnitude of this shift with approximately 135 nm is substantially larger than that reported for simple surface functionalization events (10 nm), confirming that the spectral

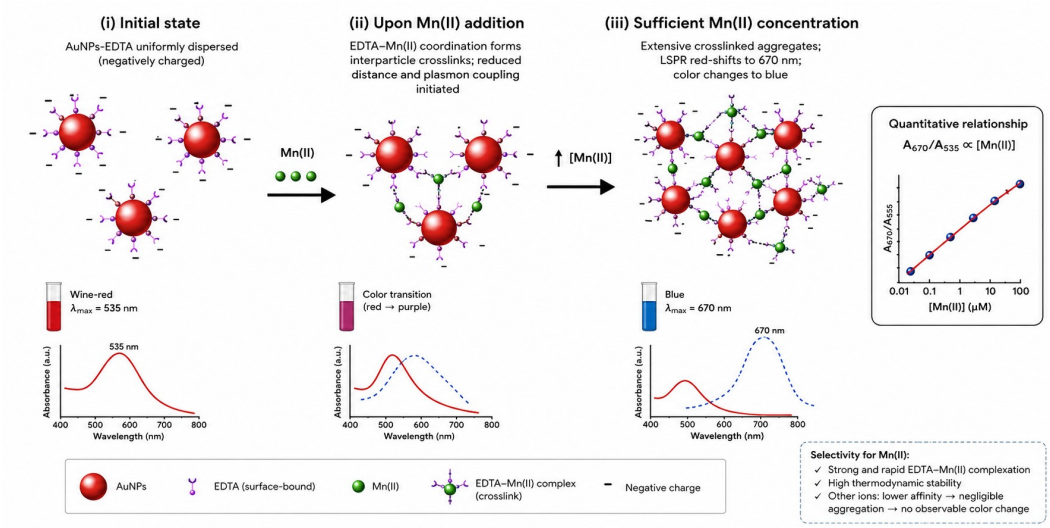

Figure 8. Schematic Illustration for Mn(II) Detection Using AuNPs-EDTA as Colorimetric Sensor Probe

change arises from genuine interparticle aggregation rather than surface perturbation (Koushki, 2021). Analogous red-shifts upon Mn(II)-induced aggregation have been documented in related nanoparticle-based sensing systems, Narayanan and Park (2014) reported a color change from red to purplish-blue for dopa-functionalized AuNPs in the presence of Mn(II), attributed to interparticle crosslinking through dopa–Mn(II) coordination; similarly, Pandey et al. (2025) reported a red-shift from 402 to 580 nm for PVP-AgNPs upon Mn(II)-induced aggregation in aqueous media.

Concomitant with the spectroscopic changes, a clear and progressive naked-eye color transition was observed in the AuNPs-EDTA colloid upon Mn(II) addition, progressing from the initial wine-red through purple and ultimately to blue as the Mn(II) concentration increased. This sequential color progression reflects the increasing degree of nanoparticle aggregation and the corresponding shift in the collective LSPR frequency of the growing aggregate clusters (Koushki, 2021; Kusuma et al., 2023). The wine-red to purple transition occurs at lower Mn(II) concentrations, corresponding to partial crosslinking and the formation of small nanoparticle dimers and trimers; the subsequent purple to blue transition at higher concentrations reflects the formation of larger, extensively crosslinked nanoparticle aggregates with dominant interparticle plasmon coupling (Kusuma et al., 2023; Sadiq et al., 2024). This characteristic tricolor progression from wine-red to purple and finally blue, is fully consistent with the well-established optical behavior of aggregating spherical AuNPs and has been reported across numerous chelating-agent-functionalized AuNP sensing systems. The reversibility and clarity of this color change enable both qualitative naked-eye screening and quantitative spectrophotometric determination of Mn(II): the absorbance ratio A_{670}/A_{535} was employed as the primary analytical signal, as it normalizes for variations in total nanoparticle concentration and provides a more robust measure of the degree of aggregation than single-wavelength absorbance alone (Kusuma et al., 2023; Saputra, 2024).

The schematic illustration of the Mn(II) detection mechanism using AuNPs-EDTA as a colorimetric probe is presented in Figure 8. The overall sensing mechanism can be summarized as a three stage process: (i) in the initial state, AuNPs-EDTA are uniformly dispersed with a negative surface charge, exhibiting wine-red coloration and an SPR peak at 535 nm; (ii) upon Mn(II) addition, rapid EDTA–Mn(II) coordination occurs, forming interparticle crosslinks that progressively reduce interparticle distance and initiate plasmon coupling; and (iii) at sufficient Mn(II) concentration, extensive crosslinked aggregates form, the LSPR band red-shifts to 670 nm, and the colloid color transitions to blue. The concentration-proportionality of the aggregation response ensures a quantitative relationship between Mn(II) concentration and the absorbance ratio A_{670}/A_{535}, forming the basis of the calibration curve for analytical quantification. This mechanism is highly selective for Mn(II) because the EDTA–Mn(II) complexation is both thermodynamically favorable and kinetically rapid under the assay conditions employed, whereas other co-existing ions exhibit substantially lower affinity for surface bound EDTA or produce aggregation responses of insufficient magnitude to generate a measurable colorimetric signal under the same conditions (Al Sheidi et al., 2024; Shakhgildyan et al., 2024).

3.5 Analytical Performance and Method Validation

The analytical performance of the developed AuNPs-EDTA colorimetric probe for Mn(II) detection was systematically evaluated in terms of linearity, sensitivity, limit of detection (LOD), limit of quantification (LOQ), selectivity, and practical applicability in spiked urine samples. These parameters are indispensable for establishing the analytical reliability, clinical relevance, and translational potential of the sensor platform. In

developing an ideal colorimetric sensor, critical performance characteristics including selectivity, sensitivity, accuracy, precision, and linearity must be rigorously assessed to confirm its suitability for quantitative analytical applications.

3.5.1 Linearity and Sensitivity

The linearity of the AuNPs-EDTA colorimetric probe for Mn(II) quantification was assessed by monitoring the absorbance ratio (A_{670}/A_{535}) as a function of Mn(II) concentration across the range of 0.5 to 7.0 μg/L. The range for urinary Mn monitoring (0.11 – 1.48 μg/L in non-exposed adults) and occupationally exposed workers of 3.8 – 4.9 μg/L. This working range was deliberately selected to encompass both physiologically appropriate background levels and elevated exposure concentrations relevant to clinical and occupational biomonitoring in biological fluids such as urine and serum (Baker et al., 2019). A strong and statistically robust linear correlation was established between the absorbance ratio and Mn(II) concentration, yielding a coefficient of determination R^2 = 0.9905 (Figure 9). This R^2 value, approaching unity, confirms that the probe response is highly proportional to Mn(II) concentration throughout the tested range, fulfilling the linearity requirement stipulated by ICH Q2(R1) guidelines for analytical method validation. The excellent linearity reflects the stoichiometric nature of the EDTA–Mn(II) crosslinking mechanism, whereby each increment in Mn(II) concentration generates a proportional increase in interparticle aggregation and a corresponding enhancement of the A_{670}/A_{535} ratio (Al Sheidi et al., 2024; Narayanan and Park, 2014).

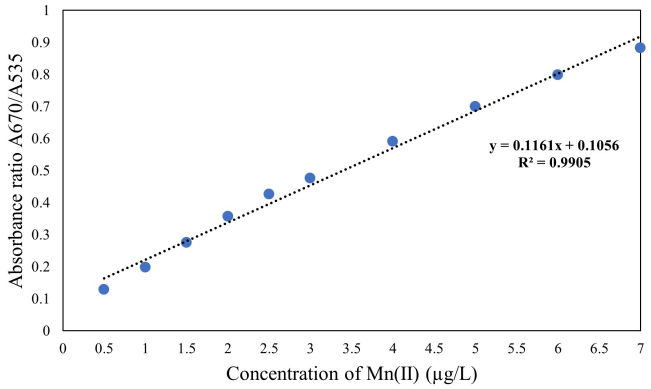

Figure 9. The Linear Calibration Curves of the Relationship Between Relative Absorbance Ratio A670/A535 and Variation of Mn(II) Concentration

The sensitivity of the assay, expressed as the slope of the calibration curve, was determined to be 0.1161 μg/L, indicating a high responsiveness of the colorimetric probe to incremental changes in Mn(II) concentration. This sensitivity value reflects the efficiency of Mn(II)-induced interparticle crosslinking: as Mn(II) concentration increases, the progressive formation of EDTA-Mn(II)-EDTA interparticle bridges amplifies the aggregation extent and consequently the plasmonic redshift, yielding a measurable and proportional increase in the A_{670}/A_{535} signal (Chen et al., 2015; Sadiq et al., 2024). The use of the absorbance ratio as the analytical signal, rather than single wavelength absorbance, provides an intrinsic normalization that improves measurement reproducibility and mitigates the influence of instrument drift and minor fluctuations in nanoparticle concentration (Saputra, 2024).

3.5.2 LOD and LOQ

The LOD and LOQ were calculated according to the IUPAC guidelines, where SD is the standard deviation of the blank response and S is the slope of the calibration curve. Calibration slope S = 0.1161 μg/L, SD blank = 0.0138 (n = 10 replicates), using the expressions LOD = 3.3 × (0.0138/0.1161) = 0.392 μg/L and LOQ = 10 × (0.0138/0.1161) = 1.189 μg/L. The LOD of the AuNPs-EDTA colorimetric sensor was determined to be 0.392 μg/L, and the LOQ was 1.189 μg/L. These low detection thresholds demonstrate that the sensor is capable of reliably detecting trace-level Mn(II) concentrations well within the physiological range of manganese in biological fluids. Specifically, the LOD of 0.392 μg/L is substantially lower than the upper reference limit for urinary manganese in unexposed individuals. Where, urinary manganese in healthy, non-occupationally exposed adults is typically reported below 1.0 μg/L (geometric mean 0.7 μg/L), frequently at or below the limit of detection, while occupationally exposed workers exhibit substantially elevated urinary Mn levels averaging 3.8-4.9 μg/L (Karyakina et al., 2022; Politis et al., 2021).

A comparative assessment of the analytical performance of the present method against recently reported Mn(II) detection methods is presented in Table 4. The comparison highlights notable differences in analytical performance and practical applicability. Several previously reported methods have demonstrated good LOD toward Mn(II), including fluorescent probes, carbon based nanomaterials, and nanoparticle based colorimetric systems. Such as colorimetric methods based on modified AuNPs from Shange et al. (2025) the LOD result was 6.9 μg/L and the method with quantum dot based fluorescence spectroscopy the LOD was 1.85 μg/L (Mohagheghpour et al., 2022; Shange et al., 2025). However, many of these platforms require specialized recognition elements, complex synthesis procedure, and primarily applied to environmental water samples rather than biological samples, particularly urine sample. In contrast, the present study employed AuNPs-EDTA, where EDTA serves not only as a stabilizing surface ligand but also as a recognition ligand for Mn(II) detection. This dual functionality simplifies sensor fabrication by integrating nanoparticle stabilization and analyte recognition within a single ligand system. Furthermore, the proposed sensor exhibits a low detection limit of 0.392 μg/L. This is well below the reference range of non-exposed adults reporting and exposed workers exhibit substantially elevated urinary Mn levels averaging 3.8-4.9 μg/L (Karyakina et al., 2022; Politis et al., 2021).

3.5.3 Selectivity

The selectivity of the AuNPs-EDTA sensor toward Mn(II) was evaluated by examining the absorbance ratio response in the presence of common co-existing cations likely to be encountered in urine and other biological matrices: Na^+, K^+, Ca^{2+}, Mg^{2+}, Zn^{2+}, Cu^{2+}, Pb^{2+}, Cd^{2+}, Co^{2+}, Ni^{2+}, Fe^{3+}, Cl^-, urea, uric acid, and creatinine. Each interferent was introduced at a concentration of 20 μg/L for metal ions and biological matrices, its four fold higher than the Mn(II) test concentration of 5.0 μg/L. The selectivity study at Figure 10, demonstrated that Mn(II) produced the highest absorbance ratio (A_{670}/A_{535}) among all tested analytes, indicating that AuNPs-EDTA exhibits a preferential response toward Mn(II). The enhanced response can be attributed to the strong affinity of EDTA toward Mn(II), which is proposed to promote more pronounced interference of the nanoparticle colloidal stability and consequently greater aggregation.

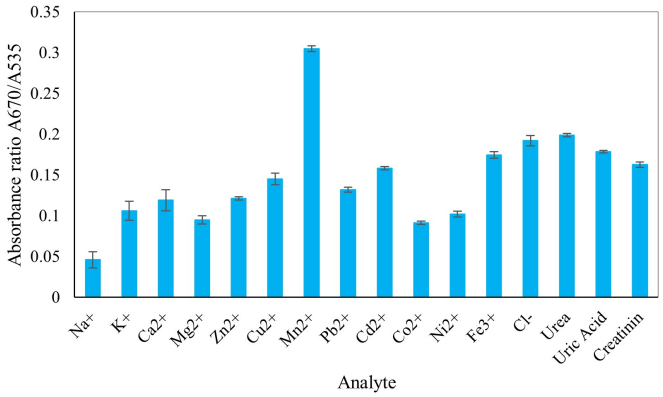

Figure 10. The Selectivity of EDTA@AuNPs for Mn(II) Detection when Compared to Differect Metal Ions (Na^+, K^+, Ca^{2+}, Mg^{2+}, Zn^{2+}, Cu^{2+}, Pb^{2+}, Cd^{2+}, Co^{2+}, Ni^{2+}, Fe^{3+}, Cl^-, Urea, Uric Acid, and Creatinine)

Several transition metal ions, like a Fe^{3+}, Cd^{2+}, and Pb^{2+}, also generated measurable responses, although their absorbance ration remained substantially lower than that observed for Mn(II). This behavior may arise from their ability to interact with EDTA ligands through coordination processes. The thermodynamically preferential coordination of EDTA with Mn(II) over the tested competing ions under the assay conditions employed, the stability constant of the Mn EDTA complex (log K = 13.79) substantially exceeds those of Na^+ and K^+ complexes, while the EDTA surface density and assay pH were optimized to minimize cross reactivity with Ca^{2+} (log K = 10.69), Mg^{2+} (log K = 8.69), and Zn^{2+} (log K = 16.50) (Al Sheidi et al., 2024). The relatively weak colorimetric response to Cu^{2+} and Zn^{2+}, may reflect steric constraints imposed by the surface-immobilized EDTA geometry that limit their crosslinking efficiency relative to Mn(II) under the specific assay conditions (Ali and Azzam, 2023; Saputra, 2024).

The interference of urinary constituents, including urea, uric acid, and creatinine, was also evaluated. Although these compounds produces change in the absorbance ratio, their responses were signifivantly lower that Mn(II), indicating that they do not strongly interfere with Mn(II) detection.

3.5.4 Application of AuNPs-EDTA for Mn(II) Detection in Spiked Urine Samples

To assess the potential of AuNPs-EDTA as a colorimetric sensor in biological samples, recovery studies were conducted using Mn(II) spiked artificial urine samples. The concentration of Mn(II) standard solution were added to urine matrix prior to analysis, and the concentrations were determined using the established calibration curve. As show in Table 5, the average recovery values were 94.46% (RSD = 0.93%) for the 1.0 μg/L spiked sample, 98.01% (RSD = 1.70%) for the 3.0 μg/L spiked sample, and 97.81% (RSD = 1.58%) fro the 5.0 μg/L. These recovery values fall within the acceptable range of 85-115% recommended by AOAC and ICH Q2 guidelines, indicating that the proposed method provides good accuracy when applied to biological matrices. In addition, the low RSD values (<2%) obtained at both concentration levels demonstrate excellent precision and reproducibility of the method. These results suggest that common urine constituents, such as electrolytes, creatinine, urea, and organic acids, do not significantly interfere with the performance of the AuNPs-EDTA sensor under the experimental conditions. Overall, the findings demonstrate that the AuNPs-EDTA colorimetric sensor has the potential to be a reliable and rapid tool for the detection of Mn(II) in urine samples.

4. CONCLUSIONS

This study successfully achieved all four stated research objectives. The first, AuNPs-EDTA with optimal physicochemical properties for colorimetric sensing were synthesized and characterized with $HAuCl_4$ concentration of 1.00 mM yielded spherical, monodisperse AuNPs (d = 20-40 nm, PDI < 0.5, SPR = 525 nm), and subsequent EDTA functionalization was confirmed by a 10 nm bathochromic SPR shift, retention of spherical morphology (d = 25-40 nm, R^2 = 0.9280), zeta potential change from -32.23 to -45.68 mV, PDI improvement to 0.36, with the FTIR spectra of EDTA immobilization (C=O at 1601.78 cm^{-1}, O−H at 3398.57 cm^{-1}, and bridging bidentate Au−O coordination confirmed via $\Delta\nu$ decrease from 199.4 to 179.9 cm^{-1}), and retention of spherical morphology (diameter 25-40 nm). Secondly, the Mn(II)-induced LSPR aggregation mechanism was fully characterized. EDTA-Mn(II)-EDTA interparticle crosslinking drives a concentration-dependent LSPR red-shift of 135 nm (535 to 670 nm) and a visible tricolor transition from wine-red through purple to blue, observable by the naked eye. Thirdly, the analytical validation confirmed excellent linearity (R^2 = 0.9905; 0.5-7.0 μg/L), a competitive LOD of 0.392 μg/L, LOQ of 1.189 μg/L, and good selectivity against co-existing urinary matrix cations (Na^+, K^+, Ca^{2+}, Mg^{2+}, Zn^{2+}, Cu^{2+}, Pb^{2+}, Cd^{2+}, Co^{2+}, Ni^{2+}, Fe^{3+}, urea, uric acid, and creatinine), demonstrating that

the AuNPs-EDTA platform achieves clinically meaningful sensitivity within the range relevant to urinary manganese biomonitoring. Fourth, the recovery values obtained from urine samples spiked with 1.0; 3.0; and 5.0 μg/L ranged from 94.46% to 98.01%, with RSD values below 2%. These results support the feasibility of using the AuNPs-EDTA colorimetric sensor for Mn(II) determination in urine samples. This work advances the field by providing, to the best of our knowledge, the first AuNPs-EDTA colorimetric sensing platform specifically designed and validated for Mn(II) detection in a urinary monitoring context, offering an instrument-independent, cost-effective, and field-deployable analytical alternative to conventional ICP-MS and AAS methods for occupational and clinical manganese surveillance. Future work should focus on validating the sensor against real clinical urine specimens from occupationally exposed populations with benchmarking against ICP-MS reference measurements, evaluating long-term colloidal stability of AuNPs-EDTA under field storage conditions, pH optimization, incubation time, and integrating the colorimetric readout with smartphone-based digital image analysis to enhance quantitative performance and accessibility for point-of-care deployment. Investigations into extending the AuNPs-EDTA platform for multiplexed detection of other occupationally relevant heavy metals are also currently underway.

5. ACKNOWLEDGEMENT

The authors gratefully acknowledge UPN Veteran Jawa Timur for providing laboratory facilities and research infrastructure that supported the completion of this study. Special thanks are extended to the Department of Chemical Engineering for access to UV-Vis spectrophotometry, and particle size analysis (PSA) instruments employed in nanoparticle characterization. The authors also thank all members of the Materials Group for their technical assistance and constructive discussions throughout this work. No conflict of interest is declared by the authors.

REFERENCES

Al Sheidi, A. S. A., L. G. Dyer, and B. Tadesse (2024). Leaching Efficacy of Ethylenediaminetetraacetic Acid (EDTA) to Extract Rare-Earth Elements from Monazite Concentrate. *Crystals*, **14**(10); 829

Ali, O. I. and A. B. Azzam (2023). Functional Ag-EDTA-Modified MnO_2 Nanocoral Reef for Rapid Removal of Hazardous Copper from Wastewater. *Environmental Science and Pollution Research*, **30**(59); 123751–123769

Alpaslan, O., A. Yaras, and H. Arslanoğlu (2020). A Kinetic Model for Chelating Extraction of Metals from Spent Hydrodesulphurization Catalyst by Complexing Agent. *Transactions of the Indian Institute of Metals*, **73**(7); 1925–1937

Amina, S. J. and B. Guo (2020). A Review on the Synthesis and Functionalization of Gold Nanoparticles as a Drug Delivery Vehicle. *International Journal of Nanomedicine*, **15**; 9823–9857

Baker, M. G., Y. S. Lin, C. D. Simpson, L. M. Shireman, S. Searles Nielsen, B. A. Racette, and N. Seixas (2019). The Reproducibility of Urinary Ions in Manganese Exposed Workers. *Journal of Trace Elements in Medicine and Biology*, **51**; 204–211

Butt, M. A., B. Imran Akca, and X. Mateos (2025). Integrated Photonic Biosensors: Enabling Next-Generation Lab-on-a-Chip Platforms. *Nanomaterials*, **15**(10); 731

Cai, B., T. Ren, X. Yu, W. Lv, and Y. Liang (2024). Aptamer-Functionalized Gold Nanoparticles for Mercury Ion Detection in a Colorimetric Assay Based on Color Change Time as Signal Readout. *Microchimica Acta*, **191**(1); 74

Chen, L., Y. Ye, H. Tan, and Y. Wang (2015). A Simple and Rapid Colorimetric Method for the Determination of Mn^{2+} Based on Pyrophosphate Modified Silver Nanoparticles. *Colloids and Surfaces A: Physicochemical and Engineering Aspects*, **478**; 1–6

Chubarov, V. M. (2023). New Approach for Direct Determination of Manganese Valence State in Ferromanganese Nodules by X-Ray Fluorescence Spectrometry. *Minerals*, **13**(10); 1329

Frens, G. (1973). Controlled Nucleation for the Regulation of the Particle Size in Monodisperse Gold Suspensions. *Nature Physical Science*, **241**(105); 20–22

Gan, Y., T. Liang, Q. Hu, L. Zhong, X. Wang, H. Wan, and P. Wang (2020). In-Situ Detection of Cadmium with Aptamer Functionalized Gold Nanoparticles Based on Smartphone-Based Colorimetric System. *Talanta*, **208**; 120231

Gusrizal, F. S. Budi, and D. Puspita (2026). Determination of Paraquat Using Microfluidic Paper-Based Analytical Device (μPAD) Immobilized with *p*-Hydroxybenzoic Acid Capped Silver Nanoparticles. *Science and Technology Indonesia*, **11**(1); 323–334

Junaidi, D. A. Malik, M. Rizki, I. Pratiwi, P. Karo-Karo, R. Marjunus, D. Asmi, and S. Hadi (2024). Synthesis of Silver Nitrate by Evaporation Chemical Reduction Process as Potential Materials for Silver Nanowires Application. *Science and Technology Indonesia*, **9**(3); 642–650

Karyakina, N. A., N. Shilnikova, N. Farhat, S. Ramoju, B. Cline, F. Momoli, D. Mattison, N. Jensen, R. Terrell, and D. Krewski (2022). Biomarkers for Occupational Manganese Exposure. *Critical Reviews in Toxicology*, **52**(8); 636–663

Kasmiati, G., R. A. Sakinah, and B. Yudono (2020). The Analysis of Manganese (Mn) in Waste Water Treatment (IPAL) of Coal Mine of PT Bukit Asam Indonesia. *Indonesian Journal of Fundamental and Applied Chemistry*, **6**(2); 53–58

Kohama, N., M. Kawahata, T. Okazaki, K. Sazawa, N. Hata, H. Kuramitz, and S. Taguchi (2025). Development of a Simple Visual and Image-Based Colorimetric Analytical Method for Mn^{2+} Using Solid-Phase Extraction with Sedimentable Dispersed Particulates. *Microchemical Journal*, **214**; 114081

Kopru, S. and M. Soylak (2024). RETRACTED ARTICLE: Inductively Coupled Plasma-Mass Spectrometry (ICP-MS) Detection of Trace Metal Contents of Children Cosmetics. *Optical and Quantum Electronics*, **56**(3); 399

Koushki, E. (2021). Effect of Conjugation with Organic Molecules on the Surface Plasmon Resonance of Gold Nanoparticles and Application in Optical Biosensing. *RSC Advances*, **11**(38); 23390–23399

Kusuma, S. A. F., J. A. Harmonis, R. Pratiwi, and A. N. Hasanah (2023). Gold Nanoparticle-Based Colorimetric Sensors: Properties and Application in Detection of Heavy Metals and Biological Molecules. *Sensors*, **23**(19); 8172

Lamothe, N., K. Elliott, Y. Pei, Y. Shi, K. Macdonald, S. J. Payne, and Z. She (2024). Electrochemical Detection of Manganese in Drinking Water with Chronoamperometry. *Electrocatalysis*, **15**(4); 353–362

Laur, N., R. Kinscherf, K. Pomytkin, L. Kaiser, O. Knes, and H.-P. Deigner (2020). ICP-MS Trace Element Analysis in Serum and Whole Blood. *PLoS One*, **15**(5); e0233357

Levy, B. S. and W. J. Nassetta (2003). Neurologic Effects of Manganese in Humans: A Review. *International Journal of Occupational and Environmental Health*, **9**(2); 153–163

Li, L. and X. Yang (2018). The Essential Element Manganese, Oxidative Stress, and Metabolic Diseases: Links and Interactions. *Oxidative Medicine and Cellular Longevity*, **2018**(1); 7580707

Mohagheghpour, E., L. Farzin, A. Ghoorchian, S. Sadjadi, and M. Abdouss (2022). Selective Detection of Manganese(II) Ions Based on the Fluorescence Turn-On Response via Histidine Functionalized Carbon Quantum Dots. *Spectrochimica Acta Part A: Molecular and Biomolecular Spectroscopy*, **279**; 121409

Nadolski, K., F. Rondepierre, C. Jonin, T. M. Goszczyński, K. Matczyszyn, and P.-F. Brevet (2023). Sensing Copper(II) Ions with Hyper Rayleigh Scattering from Gold Nanoparticles. *The Journal of Physical Chemistry C*, **127**(27); 13097–13104

Nakamoto, K. (2008). *Infrared and Raman Spectra of Inorganic and Coordination Compounds: Part A: Theory and Applications in Inorganic Chemistry*. Wiley, 1 edition

Narayanan, K. B. and H. H. Park (2014). Colorimetric Detection of Manganese(II) Ions Using Gold/Dopa Nanoparticles. *Spectrochimica Acta Part A: Molecular and Biomolecular Spectroscopy*, **131**; 132–137

Nitti, F., W. A. Ati, P. De Rozari, P. D. Ola, D. Tambaru, and L. Kadang (2023). Simple Microfluidic Paper-Based Analytical Device (μ-PAD) Coupled with Smartphone for Mn(II) Detection Using Tannin as a Green Reagent. *Indonesian Journal of Chemistry*, **23**(4); 1095

Osibe, D. A. and H. Aoyagi (2019). A Novel Strategy for the Synthesis of Gold Nanoparticles with *Catharanthus roseus* Cell Suspension Culture. *Materials Letters*, **238**; 317–320

Pandey, S., S. M. Gupta, and S. K. Sharma (2025). Detection of Manganese (II) by PVP-AgNPs for Water Monitoring. *Environmental Monitoring and Assessment*, **197**(11); 1238

Pedroso-Santana, S. and N. Fleitas-Salazar (2023). The Use of Capping Agents in the Stabilization and Functionalization of Metallic Nanoparticles for Biomedical Applications. *Particle & Particle Systems Characterization*, **40**(2); 2200146

Politis, M. D., J. C. Freedman, E. N. Haynes, and A. P. Sanders (2021). Association of Manganese Biomarker Concentrations with Blood Pressure and Kidney Parameters among Healthy Adolescents: NHANES 2013–2018. *Children*, **8**(10); 846

Potts, J. C., A. Jain, D. B. Amabilino, F. J. Rawson, and L. Pérez-García (2023). Molecular Surface Quantification of Multifunctionalized Gold Nanoparticles Using UV–Visible Absorption Spectroscopy Deconvolution. *Analytical Chemistry*, **95**(35); 12998–13002

Putri, S. A. A., S. M. Indirawati, and T. Ashar (2025). Risk Management of Manganese (Mn) Contamination in Drinking Water Sources. *Indonesian Journal of Global Health Research*, **7**(4); 471–478

Raji, S. Q. and A. T. Bader (2024). Synthesis and Characterization of Ni(II) Schiff Base Complex as a Precursor for NiO Nanoparticles and an Investigation of Their Corrosion Inhibition. *Science and Technology Indonesia*, **9**(4); 914–928

Ramzani, S., N. Khanjani, M. Mohammadyan, E. Babanezhad, and J. Yazdani-Charati (2022). Occupational Exposure to Manganese Among Welders: Association Between Airborne Manganese Concentration and Blood Manganese Levels. *Health Scope*, **11**(1)

Riyanto, S. Mardliyaliari, A. Sabrina, and M. Ridho (2025). Synthesis of Au-Pd-NPs Materials and Application as Electrochemical Sensor of Hydroquinone in Cosmetics. *Science and Technology Indonesia*, **10**(1); 294–302

Sadiq, Z., S. H. Safiabadi Tali, H. Hajimiri, M. Al-Kassawneh, and S. Jahanshahi-Anbuhi (2024). Gold Nanoparticles-Based Colorimetric Assays for Environmental Monitoring and Food Safety Evaluation. *Critical Reviews in Analytical Chemistry*, **54**(7); 2209–2244

Saffee, N., M. Shamsuddin, and K. J. Abd Karim (2019). Biosynthesized Gold Nanoparticles Supported on Magnetic Chitosan Matrix as Catalyst for Reduction of 4-Nitrophenol. *Malaysian Journal of Fundamental and Applied Sciences*, **15**(3); 451–455

Saha, K., S. S. Agasti, C. Kim, X. Li, and V. M. Rotello (2012). Gold Nanoparticles in Chemical and Biological Sensing. *Chemical Reviews*, **112**(5); 2739–2779

Saputra, E. (2024). A Colorimetric Detection of Creatinine Based-on EDTA Capped-Gold Nanoparticles (EDTA-AuNPs): Digital Image Colorimetry. *Sensors International*, **5**; 100286

Sengan, M., R. K. Kamlekar, and A. Veerappan (2020). Highly Selective Rapid Colorimetric Sensing of Pb^{2+} Ion in Water Samples and Paint Based on Metal Induced Aggregation of *N*-Decanoyltromethamine Capped Gold Nanoparticles. *Spectrochimica Acta Part A: Molecular and Biomolecular Spectroscopy*, **239**; 118485

Shakhgildyan, G., L. Avakyan, G. Atroshchenko, M. Vetchinnikov, A. Zolikova, E. Ingat'eva, M. Ziyatdinova, E. Subcheva, L. Bugaev, and V. Sigaev (2024). Ultra-Broadband Plasmon Resonance in Gold Nanoparticles Precipitated in ZnO-Al2O3-SiO2 Glass. *Chemistry and Materials Science*

Shamsuddin, M., F. Kamaludin, and S. Borhamdin (2020). Biosynthesis of Gold Nanoparticles-Peanut Shell Composite for Catalytic Reduction of Methyl Blue. *Malaysian Journal of Fundamental and Applied Sciences*, **16**(2); 252–257

Shange, S. F., P. N. Kubheka, T. R. Makhanya, P. S. Mdluli, and N. Deenadayalu (2025). Development of a Highly Selective and Sensitive Colorimetric Detection of Manganese(II) Ion in Environmental Water Using 3-(4-Hydroxy-3-Methoxyphenyl)-2,3-Dihydropyrazolo[3,4-*b*]Indole-1(4H)-Carbothioamide Modified Gold Nanoparticles: A CIE L*a*b*/Yxy Colour Space Study. *Journal of Molecular Liquids*, **427**; 127447

Sholehhudin, M., R. Azizah, A. Sumantri, S. M. Sham, Z. A. Zakaria, and M. T. Latif (2021). Analysis of Heavy Metals (cadmium, Chromium, Lead, Manganese, and Zinc) in Well Water in East Java Province. *Malaysian Journal of Medicine and Health Sciences*, **17**(2); 146–153

Sultana, E., M. Z. Rana, M. S. A. Mamun, M. Aly Saad Aly, G. E. Khedr, M. Nasiruddin, and M. Z. H. Khan (2025). Disodium EDTA-Capped AuNP-Engineered Cotton Pad as a Colorimetric Probe for Formalin Detection. *RSC Advances*, **15**(13); 10442–10452

Sutton, C. C. R., G. da Silva, and G. V. Franks (2015). Modeling the IR Spectra of Aqueous Metal Carboxylate Complexes: Correlation between Bonding Geometry and Stretching Mode Wavenumber Shifts. *Chemistry – A European Journal*, **21**(18); 6801–6805

Taha, A. and M. Shamsuddin (2014). Biosynthesis of Gold Nanoparticles Using *Psidium guajava* Leaf Extract. *Malaysian Journal of Fundamental and Applied Sciences*, **9**(3)

Takayanagi, T., K. Miyake, S. Iwasaki, D. Uehara, H. Mizuguchi, H. Okabe, and N. Matsuda (2022). Highly Stable Gold Nanoparticles in an Aqueous Solution without Any Stabilizer Prepared by a Solution Plasma Process Evaluated through Capillary Zone Electrophoresis. *Analytical Sciences*, **38**(9); 1199–1206

Turkevich, J., P. C. Stevenson, and J. Hillier (1951). A Study of the Nucleation and Growth Processes in the Synthesis of Colloidal Gold. *Discussions of the Faraday Society*, **11**; 55

Vigneshvar, S., C. Sudhakumari, B. Senthilkumaran, and H. Prakash (2016). Recent Advances in Biosensor Technology for Potential Applications–An Overview. *Frontiers in bioengineering and biotechnology*, **4**; 11

Wei, Z., A. Vandergriff, C.-H. Liu, M. Liaqat, M.-P. Nieh, Y. Lei, and J. He (2024). Strongly Coupled Plasmonic Metal Nanoparticles with Reversible pH-Responsiveness and Highly Reproducible SERS in Solution. *Nanoscale*, **16**(2); 708–718

